



Published in final edited form as:

Addict Neurosci. 2024 June ; 11: . doi:10.1016/j.addicn.2024.100153.

***Chst9* marks a spatially and transcriptionally unique population of *Oprm1*-expressing neurons in the nucleus accumbens**

Emma Andraka,

Robert A. Phillips III,

Kasey L. Brida,

Jeremy J. Day*

Department of Neurobiology, University of Alabama at Birmingham, Birmingham, AL, 35294, USA

Abstract

Opioids produce addictive, analgesic, and euphoric effects via actions at mu opioid receptors (μ ORs). The μ OR is encoded by the *Oprm1* gene and is expressed in multiple brain regions that regulate reward and motivation, such as the nucleus accumbens (NAc). *Oprm1* expression in NAc medium spiny neurons (MSNs) mediates opioid place preference, seeking, and consumption. However, recent single nucleus RNA sequencing (snRNA-seq) studies have revealed that multiple subpopulations of NAc neurons express *Oprm1* mRNA, making it unclear which populations mediate diverse behaviors resulting from μ OR activation. Using published snRNA-seq datasets from the rat NAc, we identified a novel population of MSNs that express the highest levels of *Oprm1* of any NAc cell type. Here, we show that this population is selectively marked by expression of *Chst9*, a gene encoding a carbohydrate sulfotransferase. Notably, *Chst9*⁺ neurons exhibited more abundant expression of *Oprm1* as compared to other cell types, and formed discrete cellular clusters along the medial and ventral borders of the NAc shell subregion. Moreover, *CHST9* mRNA was also found to mark specific MSN populations in published human and primate snRNA-seq studies, indicating that this unique population may be conserved across species. Together, these results identify a spatially and transcriptionally distinct NAc neuron population characterized by the expression of *Chst9*. The abundant expression of *Oprm1* in this population and the conservation of these cells across species suggests that they may play a key functional role in opioid response and identify this subpopulation as a target for further investigation.

This is an open access article under the CC BY-NC-ND license (<http://creativecommons.org/licenses/by-nc-nd/4.0/>).

*Corresponding author. jjday@uab.edu (J.J. Day).

Declaration of competing interest

The authors declare that they have no known competing financial interests or personal relationships that could have appeared to influence the work reported in this paper.

CRediT authorship contribution statement

Emma Andraka: Conceptualization, Formal analysis, Investigation, Methodology, Project administration, Writing – original draft, Writing – review & editing. **Robert A. Phillips:** Formal analysis, Investigation, Methodology, Validation, Writing – original draft, Writing – review & editing. **Kasey L. Brida:** Formal analysis, Investigation, Methodology, Writing – review & editing. **Jeremy J. Day:** Conceptualization, Formal analysis, Funding acquisition, Investigation, Project administration, Supervision, Writing – original draft, Writing – review & editing.

Supplementary materials

Supplementary material associated with this article can be found, in the online version, at [doi:10.1016/j.addicn.2024.100153](https://doi.org/10.1016/j.addicn.2024.100153).

Keywords

Nucleus accumbens; Opioids; Medium spiny neuron; Single nucleus RNA-seq

Introduction

Opioids induce rewarding and reinforcing properties by acting at endogenous opioid receptors in the central nervous system, and repeated experience with opioids can lead to physical dependence, substance use disorder, and overdose-related deaths. Endogenous and synthetic opioids activate a conserved family of $G\alpha_i$ -coupled GPCRs that include the mu, delta, and kappa opioid receptors, which are encoded by *Oprm1*, *Oprd1*, and *Oprk1*, respectively. Commonly used opioid drugs such as morphine and fentanyl produce reward via actions primarily at the mu opioid receptor (μ OR). For example, morphine conditioned place preference and dependence is lost in transgenic mice with constitutive deletion of the *Oprm1* gene [1], demonstrating that this receptor is required for opioid reward. Similarly, the μ OR plays critical roles in motivation for natural rewards and social behaviors. *Oprm1*^{-/-} mice do not increase palatable food consumption after a period of deprivation [2], and both *Oprm1*^{-/-} and *Oprm1*^{+/-} mice have impaired social interactions [3]. However, developing a complete understanding of μ OR contributions to behavior is difficult due to the broad expression of *Oprm1* in many distinct brain nuclei and cell types [4,5], each of which may contribute to distinct opioid actions.

A major target of investigation for the reward-related functions of opioids is the nucleus accumbens (NAc), a striatal subregion that integrates information about motivational states, hedonic stimuli, reward-paired cues, and contextual information [6–8]. The NAc is divided into two subregions, the core and shell. The core envelops the anterior commissure and is architecturally and functionally similar to the dorsal striatum. The NAc shell represents the most medial and ventral aspect of the NAc. While the NAc core facilitates learning and reward-related associations, the NAc shell is primarily implicated in the rewarding and reinforcing qualities of relevant stimuli [6,7,9]. Ample evidence has also demonstrated that the NAc serves as a hub for the effects of opioids on motivated behavior [5,6]. Selective restoration of *Oprm1* expression in a subset of striatal neurons in *Oprm1*^{-/-} mice rescues morphine reward, without altering the analgesic properties or withdrawal effects of morphine [10]. Likewise, direct infusions of μ OR agonists into the NAc increase food consumption [8,11], sucrose drinking [12], and intake of high-fat foods [13,14], whereas intra-NAc μ OR antagonists decrease sucrose intake and feeding behavior [15]. Additionally, opioid receptor antagonists delivered into the NAc block opioid reinforcement and social reward [16,17], and direct infusion of μ OR receptor agonists into the NAc is reinforcing in self-administration tasks [16,18,19].

The principal cells of the NAc are GABAergic medium spiny neurons (MSNs) that directly target the output nuclei of the basal ganglia (ventral tegmental area and substantia nigra) or indirectly target these nuclei through projections to the ventral pallidum [20–22]. MSNs are further separated by expression of the *Drd1* and *Drd2* dopamine receptors, which form distinct MSN populations termed D1-MSNs and D2-MSNs [23,24]. While this division is

critical for understanding striatal physiology [25], circuitry [26], and molecular responses to drugs of abuse [27–29], both cell populations express *Oprm1* [30] and contribute to opioid-induced behaviors [31]. Further, recent single nucleus RNA sequencing (snRNA-seq) studies have revealed unexpected heterogeneity in MSNs within the NAc and broader striatum, with multiple subtypes of *Drd1* and *Drd2* expressing MSNs present in the mouse [32], rat [33–35], monkey [36,37], and human NAc [37,38]. Strikingly, NAc MSN subtypes exhibit highly variable expression of *Oprm1* [34], highlighting the need for further investigation into the roles of distinct MSN subclasses in opioid action. Here, we leveraged available snRNA-seq datasets to characterize a subpopulation of NAc MSNs that exhibit the highest level of *Oprm1* expression across all defined NAc cell types. Using data-driven comparisons, we identified a marker gene (*Chst9*, which encodes a carbohydrate sulfotransferase) that defines this neuronal population. Next, we employed single molecule RNA fluorescence in situ hybridization to validate this marker and map the spatial location of this transcriptionally defined cell type in the rat NAc. Finally, comparison of transcriptional profiles of MSN subtypes from the rat, monkey, and human NAc revealed that this cell population is conserved across species. Together, these findings highlight a unique population of NAc neurons with abundant *Oprm1* expression and identify a specific molecular marker that may be useful in future targeting of this cell type.

RESULTS

Computational identification of a novel marker gene Grm8-MSNs

To begin examining subpopulations of *Oprm1*+ cells in the NAc, we first consulted a previously published snRNA-seq dataset from the rat NAc [34]. This study identified 16 transcriptionally distinct cell populations, including principal MSNs that express *Ppp1r1b* (the gene encoding dopamine- and cyclic AMP-related phosphoprotein-32, or DARPP-32; Fig. 1a–b) among other canonical MSN markers (Fig. 1d). MSN populations in the rat NAc included previously characterized D1-MSNs and D2-MSNs, as well as a novel *Ppp1r1b*+ population termed Grm8-MSNs due to enrichment of the gene *Grm8*, the gene encoding the metabotropic glutamate receptor 8 (Fig. 1c). Interestingly, *Oprm1* mRNA was highly expressed within a large proportion of Grm8-MSNs (Fig. 1d). However, we also observed less abundant *Grm8* and *Oprm1* expression in a smaller fraction of D1 and D2-MSN subpopulations (Fig. 1c–d), meaning this subpopulation cannot be distinguished by the colocalization of these genes alone.

To further investigate the unique gene expression signatures of these Grm8-MSNs, we conducted a differential expression analysis using pseudobulked gene expression matrices across 8 biological replicates. Comparing the gene expression signature of the Grm8-MSN cluster to all other cell clusters identified 223 genes enriched in the Grm8-MSN cluster and 859 genes significantly depleted in this population. Among enriched genes, *Chst9* (encoding carbohydrate sulfotransferase 9) was the most highly enriched differentially expressed gene in the Grm8-MSN population (Fig. 1e). We then assessed whether *Chst9* is selective for the Grm8-MSN cluster using the Gini coefficient, a metric useful for identifying variables not equally shared across groups or clusters of cells. This analysis identified *Chst9* as a potential marker gene for the Grm8-MSN population, as it exhibits selectively high expression for

that population only (Fig. 1f). The evaluation of *Chst9* expression within all other NAc cell populations, utilizing the same analysis pathway, confirmed this observation—every cluster outside of *Grm8*-MSNs lacked *Chst9* expression, identifying this as a unique marker gene (Fig. 1g).

Validation of *Chst9* as an *Oprm1*+ subpopulation marker gene

To validate snRNA-seq findings demonstrating that *Chst9* is in a distinct population of *Grm8*+/*Oprm1*+ MSNs in the NAc, we employed RNAscope [39], a widely implemented single molecule RNA fluorescence in situ hybridization (smRNA-FISH) platform for multiplexed transcript detection. Tissue sections containing the NAc from naïve rats were used for multiplexed hybridization using distinct probes for *Grm8*, *Oprm1*, and *Chst9* (Fig. 2a–c). Consistent with rat NAc snRNA-seq data, *Grm8*, *Oprm1*, and *Chst9* mRNA colocalized in a subset of NAc neurons (Fig. 2b–c).

Additionally, we used smRNA-FISH to visualize the spatial distribution of targeted gene transcripts. Though *Oprm1* and *Grm8* expression can be observed across the broader NAc, *Chst9* expression was restricted to a much smaller group of cells, again highlighting the selectivity of this marker across NAc subpopulations (Fig. 2c). Curiously, this *Chst9*+ population appears to form discrete cellular clusters along the medial and ventral borders of the NAc shell subregion (Fig. 2c). To confirm this observation across all animals, region of interest (ROI) coordinates from quantified cell types were combined into an integrated spatial map, forming a spatially co-registered map of cell type location of the NAc (Fig. 2d). These maps further revealed that although *Oprm1*+ cells are distributed across the medial/lateral and dorsal/ventral axes of the NAc, *Chst9*+ cells were relatively confined along the NAc shell's medial and lateral border (Fig. 2d). Additionally, by reflecting the degree of *Oprm1* expression in the area of each point, this map suggested that nearly all *Chst9*+ cells also abundantly expressed *Oprm1* (Fig. 2d).

To confirm the relative expression of *Oprm1* within different NAc cell types, we quantified the intensity and transcript-level puncta of *Oprm1* signal within all *Oprm1*+ cells. *Oprm1*+ cells were then further identified as *Chst9*+ or *Chst9*-. These analyses verified significantly elevated expression of *Oprm1* in *Chst9*+ cells as compared to *Chst9*- cells (Fig. 2e). We additionally evaluated the percentage of different NAc cell types, including *Drd1*+ and *Ppp1r1b*+ neurons, that express *Oprm1*. *Oprm1* was detected in ~40% of *Drd1*+ neurons, and in ~30% of total NAc cells (Fig. 2f). However, *Oprm1* is expressed in over 90% of *Chst9*+ NAc neurons (Fig. 2f). In combination with snRNA-seq data, these observations confirm *Chst9* as a selective marker for NAc neurons that abundantly express *Oprm1* mRNA.

Conservation of *Chst9*+ neurons across mammalian species

While these studies identify *Chst9*+ MSNs in the rat brain, we next investigated conservation of this NAc cell population across species, with a focus on higher-order mammals. To do this, we leveraged publicly available snRNA-seq atlases of the non-human primate (NHP) [36] and human [38] NAc that have previously been used to compare gene expression profiles and MSN subtypes across species [34]. As previously described, both NHP and

human datasets identified unique MSN clusters that exhibit similar marker gene expression patterns to those observed in the rat NAc (Fig. 3a–c). The direct comparison of *Grm8*, *Oprm1*, and *Chst9* expression between these species revealed that one cell type in each respective dataset exhibited colocalization and abundant expression of both *Grm8/GRM8* and *Oprm1/OPRM1*. Notably, the same population was marked by cluster-selective *Chst9/CHST9* expression. While the rat literature had termed these populations Grm8-MSNs, NHP datasets termed them D1-NUDAP cells, and human datasets referred to these as MSN.D1_F cells (Fig. 3a–c).

Transcriptionally conserved cell types should be expected to display a similar enrichment and co-expression of other marker genes as well. To examine whether this was the case, we generated co-expression heatmaps of selected transcripts within Grm8-MSNs, D1-NUDAP cells, and MSN.D1_F cells (Fig. 3d–f). For this analysis, we prioritized previously characterized markers of MSNs or MSN subtypes, in addition to *Grm8*, *Chst9*, and *Oprm1*. Consistent with a potentially conserved role across rodent and primate NAc samples, we observed similar patterns of expression for additional marker genes in these populations. For example, each cluster included a high percentage of cells expressing the genes *Foxp2* and *Bcl11b*, commonly cited markers of MSNs [40,41]. Furthermore, an appreciable subset of cells in each cluster expressed *Drd1/DRD1* and *Pdyn/PDYN*, both established markers of D1-MSNs [42, 43]. Additionally, feature expression plots from each species confirmed a similar expression of *Drd1/DRD1*, among other genes, across these three clusters (Fig. S1). Taken together, this finding demonstrates that Grm8-MSNs, and specifically *Chst9+* neurons, are conserved across species and exhibit similar gene expression signatures to previously described cell types in higher-order mammals.

Discussion

Recent large-scale single cell sequencing platforms have enabled comprehensive dissection of the molecular architecture of the striatum (including the NAc) in Multiple species [32–36,38]. While these efforts have identified transcriptionally distinct subdivisions within larger D1-MSN and D2-MSN subclasses, the convergence of cell types and the reliability of specific marker genes across species remains unclear. Here, we leveraged published snRNA-seq datasets from the rat NAc to identify putative transcriptional markers of Grm8-MSNs, a poorly characterized population of neurons that has been identified in multiple rodent snRNA-seq datasets across different laboratories [33–35,44]. Notably, this cell population exhibits the highest expression of *Oprm1* within the NAc, and is selectively marked by mRNA for the carbohydrate sulfotransferase gene *Chst9*. At an anatomical level, *Chst9+* MSNs populate the ventral and medial borders of the NAc shell subregion, where they localize in discrete clusters that co-express *Grm8*. Moreover, we demonstrate that *Chst9+* cells are observed in NAc subpopulations in the monkey and human NAc, providing evidence for a conserved transcriptional profile. Together, these results help to define a poorly characterized cell type in the NAc, and highlight the need for further investigation into the circuit and behavioral role of *Chst9+* MSNs.

The anatomical localization of *Chst9+* MSNs at the border of the rat NAc may generate confusion given the proximity to other nearby landmarks, including the Islands of Calleja

and anterior components of the ventral pallidum that perforate the ventral NAc shell. Fortunately, these distinct nuclei can be reliably distinguished from principal NAc neurons at the molecular level. For example, the Islands of Calleja are densely organized pockets of granule cells within the ventral striatum, which play a key role in grooming behavior [45]. While the Islands of Calleja can easily be localized in a coronal section based on cell density alone (e.g., increased DAPI+ territories in Fig. 2a), they are also marked by robust expression of the *Drd3* receptor [45], which is largely absent in *Chst9+* MSNs. Likewise, *Chst9+* MSNs do not express other markers of ventral pallidum neuronal subtypes, including *Npas1* and *Pvalb* [46,47], but do express appreciable levels of D1-MSN markers including *Drd1*, *Bcl11b*, *Pdyn*, and *Ppp1r1b*. Together with molecular conservation in higher-order mammals, these results argue that *Chst9+* MSNs represent a distinct cell type that is both transcriptionally and anatomically separate from other defined MSN subtypes [34,36].

Strong evidence supports a critical role of μ ORs in the NAc in the rewarding and reinforcing properties of opioids. However, the specific contributions of distinct cell types or anatomical subregions is only beginning to be understood. Landmark studies previously identified “hotspots” for opioid effects on hedonic reactions to sucrose reward, as defined by enhancement of orofacial affective taste reactivity measures [8,11,48,49]. These studies outlined a rostradorsal domain of the medial NAc shell as having the most robust effects in stimulating “liking” of palatable rewards, whereas μ OR activation in other regions of the NAc produced more moderate effects or even generated food avoidance. Notably, the strongest hedonic effects of μ OR activation at least partially overlap with the distribution of *Chst9+* clusters in the NAc shell (Fig. 2d), suggesting a possible role for these cells in hedonic reactions to palatable foods. Given the abundant expression of *Oprm1* in *Chst9+* cells and the high fraction of *Chst9+* cells that express *Oprm1*, it would be a reasonable assumption that these cells would be among the most responsive to μ OR activation. Prior evidence from *Fos* plume mapping following direct NAc microinfusions of μ OR agonists identified dose-dependent elevations in FOS protein [11,14,49], but the molecular identity of FOS+ cells was not investigated. Similarly, an early single cell RNA-seq investigation revealed increased activity-driven gene expression in a small subset of D1-MSNs after morphine exposure in a mouse model [50], although it is unclear if these changes were confined to a distinct subset of D1-MSNs. Likewise, a recent study found no change in *Fos* (or related AP-1 transcription factor family member *Fosb*) in Grm8-MSNs following either single or repeated cocaine administration [34]. Future studies will be needed to comprehensively define the electrophysiological and transcriptional responses of *Chst9+* cells to opioids and other psychoactive drugs.

Although we identified *Chst9* as the most specific marker for Grm8-MSNs, we also detected elevated levels of other potential marker genes in this population (Fig. 1e). These included *Tshz1* (Teashirt zinc finger homeobox 1) and *Tac3* (Tachykinin precursor 3; the rat ortholog of mouse *Tac2*). Each of these genes have recently been discovered by other groups to mark specific populations of MSNs in the dorsal and ventral striatum, and cells expressing these genes have been shown to be important for aversive aspects of motivated behavior [43,51]. *Tshz1* is expressed by a subgroup of striosomal D1-MSNs located in the dorsal striatum, but is also found in the ventral striatum. Notably, *Tshz1+* neurons in the dorsal striatum are activated by aversive stimuli, and optogenetic stimulation of these cells causes place aversive

and suppresses locomotion [43]. Similarly, inhibiting *Tshz1*+ MSNs impairs learning related to punishment, but does not impact reward learning. However, while this study characterized *Tshz1*+ MSNs in the dorsal striatum, nothing is known about the behavioral role of *Tshz1*+ neurons in the ventral striatum or NAc, and we did not observe significant *Chst9* expression in the dorsal striatum. Similarly, another recent study identified *Tac2* mRNA to mark a subpopulation of D1-MSNs in the mouse NAc [51]. This study found that acute cocaine decreased activity of *Tac2*+ neurons, and stimulation of this population suppressed cocaine place preference and self-administration. Given the enrichment of *Tac3* in rat Grm8-MSNs, the cells targeted in this mouse study likely overlap to some extent with the *Chst9*+ cells investigated in the present manuscript. However, further work is needed to characterize the circuit and behavioral role of this population, including synaptic inputs and downstream targets.

In summary, we have identified a transcriptionally and anatomically unique population of NAc MSNs marked by high expression of *Oprm1* and selective expression of *Chst9*. Given that this population expresses other markers of D1-MSNs, it is likely that prior labeling studies or genetic manipulations may have targeted this cell population along with more classically defined D1-MSNs that do not express *Chst9* and exhibit lower expression of *Oprm1*. For example, use of *Drd1* or prodynorphin (*Pdyn*) gene promoter sequences is a common strategy for cell-restricted expression of transgenes in D1-MSNs [2,21,52–54]. Using this strategy, prior work has revealed that *Oprm1* expression in *Pdyn*+ cells (using a *Pdyn* BAC transgenic mouse) is sufficient to restore opioid reward in an *Oprm1*^{-/-} mouse [10]. However, based on the present results (as well as recent work demonstrating that *Pdyn* regulatory elements are accessible in Grm8-MSNs [55]), it is likely that this manipulation restores *Oprm1* expression in multiple MSN subtypes including *Chst9*+ cells, which may each contribute to opioid reward in distinct ways. Our results highlight the previously underappreciated diversity within broad striatal MSN subclasses, and underline the need for continued exploration of the distinct roles of unique cell types.

Materials and methods

Animals

Adult male and female Sprague-Dawley rats were obtained from Charles River Laboratories (Wilmington, MA, USA). Rats were cohoused in pairs in plastic filtered cages with nesting enrichment in an Association for Assessment and Accreditation of Laboratory Animal Care–approved animal care facility maintained between 22° and 24 °C on a 12-hour light/12-hour dark cycle with ad libitum food (Lab Diet Irradiated rat chow) and water. Bedding and enrichment were changed weekly by animal resources program staff. A total of 6 naïve rats ($n = 3$ M/3F) were used in initial *Chst9* population and MSN characterization experiments. Animals were randomly assigned to experimental groups. All experiments were approved by the University of Alabama at Birmingham Institutional Animal Care and Use Committee (IACUC).

Brain tissue collection

Rats were euthanized by live decapitation using a guillotine (World Precision Instruments, Sarasota, FL, USA). Brains were rapidly removed and submerged in 2-methylbutane, chilled on dry ice, for approximately 30 s. Flash-frozen brains were then wrapped in aluminum foil and placed on dry ice. Tissue was stored at -80°C until the day of sectioning. After a 30-minute equilibration at -20°C , $10\ \mu\text{m}$ coronal sections were obtained using a Leica CM 1850 cryostat (Deer Park, IL, USA) set to -20°C . Sections containing the NAc, ranging from 1.68 to 1.92 mm anterior-posterior (A/P) to Bregma, were mounted onto room temperature frosted microscope slides, air dried for 60 min at -20°C , and stored at -80°C until staining.

Tissue preparation and imaging for RNAscope

The RNAscope Multiplex Fluorescent v2 assay kit (ACD Bio, 323,110) and RNAscope 4-plex ancillary kit (ACD Bio, 323,120) were used to stain sections, following the manufacturer's recommended protocol. Probe sets used include DAPI (320,858), Rn-Oprm1-C1 mRNA (410,691-C1), Rn-Grm8-C2 mRNA (1,149,671-C2), Rn-Chst9-C4 mRNA (1,149,681-C4), Rn-Ppp1r1b-C2 mRNA (1,048,941-C2), and Rn-Drd1-C3 mRNA (317,031-C3). Three different groups of sections were probed, with varying marker probe combinations—group 1 (*Chst9* population validation experiment) probes included *Oprm1*, *Grm8*, and *Chst9*; group 2 (MSN marker experiment) probes included *Oprm1*, *Ppp1r1b*, and *Drd1*; group 3 (MSN marker experiment) probes included *Oprm1*, *Ppp1r1b*, and *Chst9*. Channels were matched with genes according to relative expression level and channel background in different experiments: the green channel (520 nm dye, recommended for high expressors) was assigned to *Grm8*, *Ppp1r1b*, and *Oprm1*, the red channel (570 nm dye, recommended for low expressors) was assigned to *Oprm1*, and the white channel (690 nm dye, recommended for low expressors) was assigned to *Chst9* and *Drd1*. 5 total sections (1 each from 3 M/2F) were used for the *Chst9* population validation experiment, and 6 total sections (1 each from 3 M/3F) were used for each of the MSN marker experiment. After staining, sections were imaged using the BZ-X800 Keyence Microscope, and then stitched using the BZ-X800 Keyence Analyzer software. High sensitivity images were taken using OP-87,767 filter cubes for GFP (Channel 1, green), Texas Red (PE) (Channel 2, red), DAPI (Channel 3, blue) and Cy5 (Channel 4, white) at 4x (PlanApo NA 0.20), 20x (Plan Fluor NA 0.45 Ph1), and 100x (PlanApo 1.45/0.113 mm Oil) magnifications.

Image analysis

Approximate A/P coordinates of sections were determined by comparing anatomical landmarks within 4x whole section images to those in coordinate and region-labeled diagrams of the Paxinos and Watson rat brain atlas [56]. These A/P distinctions were used to process 20x ROI images of the NAc. This protocol was used for the *Chst9* population validation and MSN marker experiments. To isolate the NAc for quantification, brain atlas templates at the corresponding A/P coordinate to that of a given section were overlaid on 20x images of that section in Adobe Illustrator (San Jose, CA, USA) using anatomical landmarks as a guide. This overlay image was then imported into FIJI [57] to create NAc-specific ROIs for that 20x image. These ROIs were then applied to each individual channel

of the original 20x image, and the NAc was cropped from the rest of each channel's image using the Clear Outside plugin. DAPI channel nuclei-specific ROIs were generated with the StarDist-2D plugin [58], using the "Versatile (fluorescent nuclei)" model with a probability/score threshold of 0.20 and an overlap threshold of 0.45. Nuclei-specific ROIs were then applied to images containing *Oprm1*, *Grm8*, *Chst9*, *Ppp1r1b*, or *Drd1* probe signal, and raw signal intensity within each ROI was measured. Cell types were categorized based on positive marker colocalization within a single ROI, and intensity values were determined within different cell types, using R Studio. Nuclei-specific ROI positions were used to plot locations of different cell types, using R Studio.

100x magnification images were taken using the z-stack setting. One image for each channel within a stack was chosen for analysis, for a total of 10–14 images per animal within the *Chst9* population validation experiment. Selected channel images for one total z-stack image were merged, and the resulting overlay was converted to Nikon (.nd2) format using NIS-Elements software. Nuclei-specific ROIs were generated around DAPI staining using QuPath [59] software version 0.3.2. Cell detection parameters were set to background radius 0 px, median filter radius 0 px, minimum area 100 px², maximum area 3000 px², threshold 35, and cell expansion 3 px. For cell detection, "split by shape", "include cell nucleus", "smooth boundaries", and "make measurements" boxes were checked. Marker puncta-specific ROIs were then generated, and counts were measured within each DAPI ROI for an image. Subcellular detection parameters were set to expected spot size 12 px², minimum spot size 0.5 px², and maximum spot size 25 px². Cell types were categorized based on positive marker colocalization within a single ROI, and puncta counts were determined within different cell types, using R Studio.

Statistical analysis

All image data were analyzed statistically with Prism software using the nested *t*-test (*Chst9* population validation experiment). A 95% confidence level was set for every test, with a definition of statistical significance at $p < 0.05$. All graphs, diagrams, and image edits were made using Prism, Adobe Illustrator, R Studio, and FIJI.

Published snRNA-seq data analysis

Data objects for NHP and human NAc snRNA-seq datasets were obtained from data repositories outlined in each respective publication. The data object for the rat NAc snRNA-seq dataset was provided directly by Robert Phillips at the University of Alabama at Birmingham (UAB). All data objects were analyzed with R software. Data for *Grm8*, *Oprm1*, *Chst9*, *Ppp1r1b*, and *Drd1* expression were obtained in the form of UMAP cluster plots and violin plots through Seurat [60], ggplot2, and dplyr package processing in R Studio.

Supplementary Material

Refer to Web version on PubMed Central for supplementary material.

Acknowledgements

We thank all current and former Day Lab members for assistance and support. This work was supported by NIH grants DP1DA039650, R01MH114990, R01DA053743, R01DA054714, and the McKnight Foundation Neurobiology of Brain Disorders Award (JJ). R.A.P.III is supported by the AMC21 scholar program and the UAB T32 in the Neurobiology of Cognition and Cognitive Disorders (T32NS061788). We acknowledge support from the University of Alabama at Birmingham Biological Data Science Core (RRID:SCR_021766), and the UAB Heflin Center for Genomic Sciences.

Data availability

Data will be made available on request.

References

- [1]. Matthes HW, et al. , Loss of morphine-induced analgesia, reward effect and withdrawal symptoms in mice lacking the mu-opioid-receptor gene, *Nature* 383 (1996) 819–823. [PubMed: 8893006]
- [2]. Castro DC, et al. , An endogenous opioid circuit determines state-dependent reward consumption, *Nature* 598 (2021) 646–651. [PubMed: 34646022]
- [3]. Toddes C, Lefevre EM, Brandner DD, Zugschwert L, Rothwell PE, μ -opioid receptor (Oprm1) copy number influences nucleus accumbens microcircuitry and reciprocal social behaviors, *J. Neurosci* 41 (2021) 7965–7977. [PubMed: 34301826]
- [4]. Erbs E, et al. , A mu-delta opioid receptor brain atlas reveals neuronal co-occurrence in subcortical networks, *Brain Struct. Funct* 220 (2015) 677–702. [PubMed: 24623156]
- [5]. Le Merrer J, Becker JAJ, Befort K, L Kieffer B, Reward processing by the opioid system in the brain, *Physiol. Rev* 89 (2009) 1379–1412. [PubMed: 19789384]
- [6]. Castro DC, A Motivational Bruchas MR, Neuropeptidergic Hub, Anatomical and functional diversity within the nucleus accumbens shell, *Neuron* 102 (2019) 529–552. [PubMed: 31071288]
- [7]. Day JJ, Carelli RM, The nucleus accumbens and Pavlovian reward learning, *Neuroscientist* 13 (2007) 148–159. [PubMed: 17404375]
- [8]. Peciña S, Berridge KC, Hedonic hot spot in nucleus accumbens shell: where do mu-opioids cause increased hedonic impact of sweetness? *J. Neurosci* 25 (2005) 11777–11786. [PubMed: 16354936]
- [9]. Loriaux AL, Roitman JD, Roitman MF, Nucleus accumbens shell, but not core, tracks motivational value of salt, *J. Neurophysiol* 106 (2011) 1537–1544. [PubMed: 21697439]
- [10]. Cui Y, et al. , Targeted expression of μ -opioid receptors in a subset of striatal direct-pathway neurons restores opiate reward, *Nat. Neurosci* 17 (2014) 254–261. [PubMed: 24413699]
- [11]. Peciña S, Berridge KC, Opioid site in nucleus accumbens shell mediates eating and hedonic “liking” for food: map based on microinjection Fos plumes, *Brain Res* 863 (2000) 71–86. [PubMed: 10773195]
- [12]. Zhang M, Kelley AE, Opiate agonists microinjected into the nucleus accumbens enhance sucrose drinking in rats, *Psychopharmacology (Berl.)* 132 (1997) 350–360. [PubMed: 9298512]
- [13]. Zhang M, Gosnell BA, E Kelley A, Intake of high-fat food is selectively enhanced by mu opioid receptor stimulation within the nucleus accumbens, *J. Pharmacol. Exp. Ther* 285 (1998) 908–914. [PubMed: 9580643]
- [14]. Zhang M, Kelley AE, Enhanced intake of high-fat food following striatal mu-opioid stimulation: microinjection mapping and fos expression, *Neuroscience* 99 (2000) 267–277. [PubMed: 10938432]
- [15]. Kelley AE, Bless EP, J Swanson C, Investigation of the effects of opiate antagonists infused into the nucleus accumbens on feeding and sucrose drinking in rats, *J. Pharmacol. Exp. Ther* 278 (1996) 1499–1507. [PubMed: 8819538]
- [16]. van Ree JM, Gerrits MA, Vanderschuren LJ, Opioids reward and addiction: an encounter of biology, psychology, and medicine, *Pharmacol. Rev* 51 (1999) 341–396. [PubMed: 10353987]

- [17]. Trezza V, Damsteegt R, Achterberg EJM, Vanderschuren LJMJ, Nucleus accumbens μ -opioid receptors mediate social reward, *J. Neurosci* 31 (2011) 6362–6370. [PubMed: 21525276]
- [18]. David V, Cazala P, Anatomical and pharmacological specificity of the rewarding effect elicited by microinjections of morphine into the nucleus accumbens of mice, *Psychopharmacology (Berl.)* 150 (2000) 24–34. [PubMed: 10867973]
- [19]. Olds ME, Reinforcing effects of morphine in the nucleus accumbens, *Brain Res* 237 (1982) 429–440. [PubMed: 7083004]
- [20]. Pardo-Garcia TR, et al. , Ventral pallidum is the primary target for accumbens D1 projections driving cocaine seeking, *J. Neurosci* 39 (2019) 2041–2051. [PubMed: 30622165]
- [21]. Kupchik YM, et al. , Coding the direct/indirect pathways by D1 and D2 receptors is not valid for accumbens projections, *Nat. Neurosci* 18 (2015) 1230–1232. [PubMed: 26214370]
- [22]. Baimel C, McGarry LM, G Carter A, The projection targets of medium spiny neurons govern cocaine-evoked synaptic plasticity in the nucleus accumbens, *Cell Rep* 28 (2019) 2256–2263.e3. [PubMed: 31461643]
- [23]. Le Moine C, Bloch B, D1 and D2 dopamine receptor gene expression in the rat striatum: sensitive cRNA probes demonstrate prominent segregation of D1 and D2 mRNAs in distinct neuronal populations of the dorsal and ventral striatum, *J. Comp. Neurol* 355 (1995) 418–426. [PubMed: 7636023]
- [24]. Gerfen CR, Segregation of D1 and D2 dopamine receptors in the striatal direct and indirect pathways: an historical perspective, *Front. Synaptic Neurosci* 14 (2022) 1002960. [PubMed: 36741471]
- [25]. Shen W, Flajolet M, Greengard P, Surmeier DJ, Dichotomous dopaminergic control of striatal synaptic plasticity, *Science* 321 (2008) 848–851. [PubMed: 18687967]
- [26]. Park J, Coddington LT, T Dudman J, Basal ganglia circuits for action specification, *Annu. Rev. Neurosci* 43 (2020) 485–507. [PubMed: 32303147]
- [27]. Calipari ES, et al. , In vivo imaging identifies temporal signature of D1 and D2 medium spiny neurons in cocaine reward, *Proc. Natl. Acad. Sci. USA* 113 (2016) 2726–2731. [PubMed: 26831103]
- [28]. Thibeault KC, Kutlu MG, Sanders C, Calipari ES, Cell-type and projection-specific dopaminergic encoding of aversive stimuli in addiction, *Brain Res* 1713 (2019) 1–15. [PubMed: 30580012]
- [29]. Bertran-Gonzalez J, et al. , Opposing patterns of signaling activation in dopamine D1 and D2 receptor-expressing striatal neurons in response to cocaine and haloperidol, *J. Neurosci* 28 (2008) 5671–5685. [PubMed: 18509028]
- [30]. Oude Ophuis RJA, Boender AJ, van Rozen AJ, Adan RAH, Cannabinoid, melanocortin and opioid receptor expression on DRD1 and DRD2 subpopulations in rat striatum, *Front. Neuroanat* 8 (2014) 14. [PubMed: 24723856]
- [31]. Severino AL, et al. , μ -Opioid receptors on distinct neuronal populations mediate different aspects of opioid reward-related behaviors, *eNeuro* 7 (2020).
- [32]. Chen R, et al. , Decoding molecular and cellular heterogeneity of mouse nucleus accumbens, *Nat. Neurosci* 24 (2021) 1757–1771. [PubMed: 34663959]
- [33]. Savell KE, et al. , A dopamine-induced gene expression signature regulates neuronal function and cocaine response, *Sci. Adv* 6 (2020) eaba4221. [PubMed: 32637607]
- [34]. Phillips RA, et al. , Distinct subpopulations of D1 medium spiny neurons exhibit unique transcriptional responsiveness to cocaine, *Mol. Cell. Neurosci* 125 (2023) 103849. [PubMed: 36965548]
- [35]. Reiner BC, et al. , Single nucleus transcriptomic analysis of rat nucleus accumbens reveals cell type-specific patterns of gene expression associated with volitional morphine intake, *Transl. Psychiatry* 12 (2022) 374. [PubMed: 36075888]
- [36]. He J, et al. , Transcriptional and anatomical diversity of medium spiny neurons in the primate striatum, *Curr. Biol* 31 (2021) 5473–5486.e6. [PubMed: 34727523]
- [37]. Phan BN, et al. , Single nucleus transcriptomics of human and monkey striatum implicates DNA damage, neuroinflammation, and neurodegeneration signaling in opioid use disorder, *BioRxiv* (2023), 10.1101/2023.05.17.541145.

- [38]. Tran MN, et al. , Single-nucleus transcriptome analysis reveals cell-type-specific molecular signatures across reward circuitry in the human brain, *Neuron* 109 (2021) 3088–3103.e5. [PubMed: 34582785]
- [39]. Wang F, et al. , RNAscope: a novel in situ RNA analysis platform for formalin-fixed, paraffin-embedded tissues, *J Mol Diagn* 14 (2012) 22–29. [PubMed: 22166544]
- [40]. Arlotta P, Molyneaux BJ, Jabaudon D, Yoshida Y, D Macklis J, Ctip2 controls the differentiation of medium spiny neurons and the establishment of the cellular architecture of the striatum, *J. Neurosci* 28 (2008) 622–632. [PubMed: 18199763]
- [41]. Cirnaru M-D, et al. , Unbiased identification of novel transcription factors in striatal compartmentation and striosome maturation, *Elife* 10 (2021).
- [42]. Gerfen CR, et al. , D1 and D2 dopamine receptor-regulated gene expression of striatonigral and striatopallidal neurons, *Science* 250 (1990) 1429–1432. [PubMed: 2147780]
- [43]. Xiao X, et al. , A genetically defined compartmentalized striatal direct pathway for negative reinforcement, *Cell* 183 (2020) 211–227.e20. [PubMed: 32937106]
- [44]. Hughes BW, et al. , NPAS4 supports drug-cue associations and relapse-like behavior through regulation of the cell type-specific activation balance in the nucleus accumbens, *BioRxiv* (2022), 10.1101/2022.09.04.506434.
- [45]. Zhang Y-F, et al. , Ventral striatal islands of Calleja neurons control grooming in mice, *Nat. Neurosci* 24 (2021) 1699–1710. [PubMed: 34795450]
- [46]. Morais-Silva G, et al. , Molecular, circuit, and stress response characterization of Ventral Pallidum Npas1-neurons, *J. Neurosci* (2022), 10.1523/JNEUROSCI.0971-22.2022.
- [47]. Cui Q, et al. , Dissociable roles of pallidal neuron subtypes in regulating motor patterns, *J. Neurosci* (2021), 10.1523/JNEUROSCI.2210-20.2021.
- [48]. Castro DC, Berridge KC, Opioid hedonic hotspot in nucleus accumbens shell: mu, delta, and kappa maps for enhancement of sweetness “liking” and “wanting, *J. Neurosci* 34 (2014) 4239–4250. [PubMed: 24647944]
- [49]. Peciña S, Smith KS, Berridge KC, Hedonic hot spots in the brain, *Neuroscientist* 12 (2006) 500–511. [PubMed: 17079516]
- [50]. Avey D, et al. , Single-cell RNA-seq uncovers a robust transcriptional response to morphine by glia, *Cell Rep* 24 (2018) 3619–3629.e4. [PubMed: 30257220]
- [51]. Zhao Z-D, et al. , A molecularly defined D1 medium spiny neuron subtype negatively regulates cocaine addiction, *Sci. Adv* 8 (2022) eabn3552. [PubMed: 35960793]
- [52]. Gong S, et al. , A gene expression atlas of the central nervous system based on bacterial artificial chromosomes, *Nature* 425 (2003) 917–925. [PubMed: 14586460]
- [53]. Shuen JA, Chen M, Gloss B, & Calakos N *Drd1a-tdTomato* BAC transgenic mice for simultaneous visualization of medium spiny neurons in the direct and indirect pathways of the basal ganglia, *J. Neurosci* 28 (2008) 2681–2685. [PubMed: 18337395]
- [54]. Pettibone JR, et al. , Knock-In Rat Lines with Cre Recombinase at the Dopamine D1 and Adenosine 2a Receptor Loci, *eNeuro* 6 (2019).
- [55]. Phillips RA, et al. , Temporally specific gene expression and chromatin remodeling programs regulate a conserved Pdyn enhancer, *BioRxiv* (2023), 10.1101/2023.06.02.543489.
- [56]. Paxinos G, Watson C, *The Rat Brain in Stereotaxic Coordinates*, 472, Academic Press, 2013.
- [57]. Schindelin J, et al. , Fiji: an open-source platform for biological-image analysis, *Nat. Methods* 9 (2012) 676–682. [PubMed: 22743772]
- [58]. Schmidt U, Weigert M, Broaddus C, Myers G, in: Frangi AF, Schnabel JA, Davatzikos C, Alberola-López C, Fichtinger G (Eds.), *Medical Image Computing and Computer Assisted Intervention – MICCAI2018: 21st International Conference, Granada, Spain, September 16–20, 2018, Proceedings, Part II* 11071, Springer International Publishing, 2018, pp. 265–273.
- [59]. Bankhead P, et al. , QuPath: open source software for digital pathology image analysis, *Sci. Rep* 7 (2017) 16878. [PubMed: 29203879]
- [60]. Butler A, Hoffman P, Smibert P, Papalexi E, Satija R, Integrating single-cell transcriptomic data across different conditions, technologies, and species, *Nat. Biotechnol* 36 (2018) 411–420. [PubMed: 29608179]

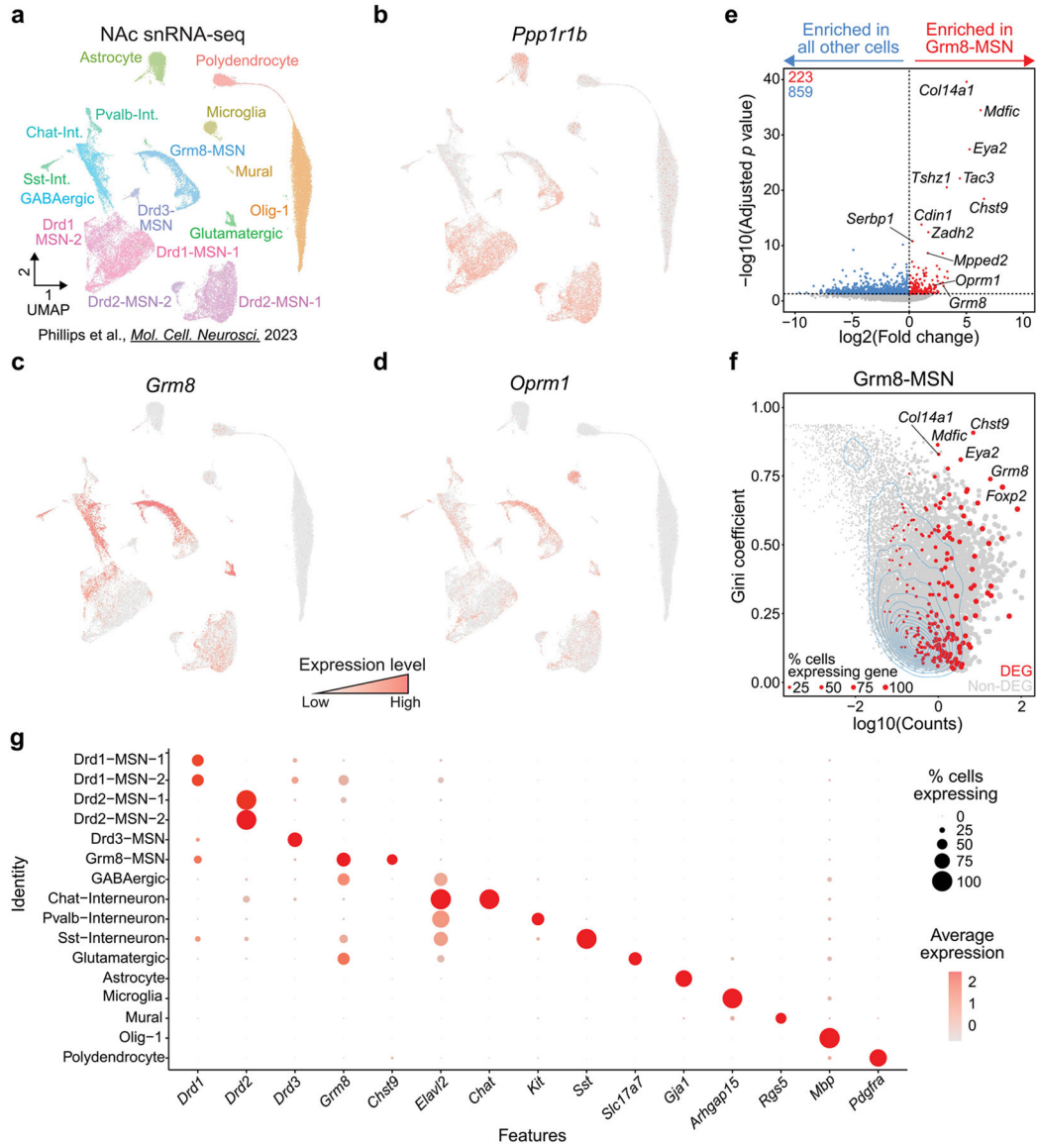


Fig. 1. Identification of *Chst9* as a marker gene for Grm8-MSNs. **a**, UMAP of previously published snRNA-seq data from NAc of male and female Sprague-Dawley rats identifies 16 transcriptionally distinct cell populations. **b-d**, Feature plots showing distribution of genes expressed in Grm8-MSNs, including *Ppp1r1b* (a pan-MSN marker), *Grm8*, and *Oprm1*. **e**, Volcano plot for identification of differentially expressed genes enriched in Grm8-MSNs. **f**, Gini coefficient analysis identifies *Chst9* as a marker gene with high and selective expression in Grm8-MSNs. **g**, Dot plot for identified marker genes for identified cell populations.

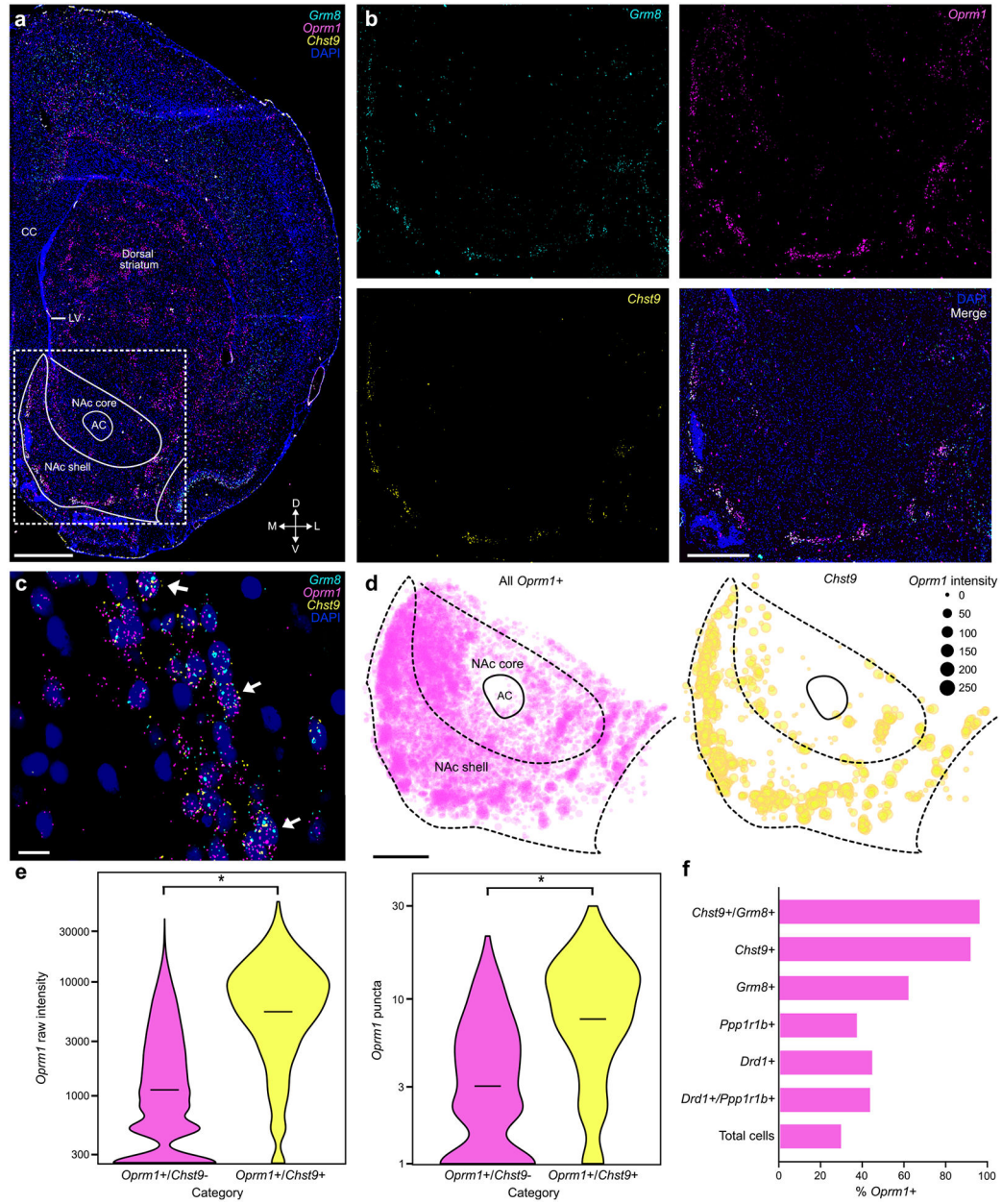


Fig. 2. Validation of *Oprm1* subpopulation marker genes with multiplexed RNAscope single molecule RNA-FISH. **a**, Representative 4x image of *Grm8* (cyan), *Oprm1* (magenta), *Chst9* (yellow), and DAPI (blue) detection in a rat brain section with annotated anatomical landmarks. CC, corpus callosum; LV, lateral ventricle; AC, anterior commissure. Scale bar, 1 mm. **b**, Representative 20x images of *Oprm1*, *Grm8*, *Chst9*, and DAPI in the NAc. Scale bar, 500 μ m. **c**, Identification of *Grm8*⁺/*Oprm1*⁺/*Chst9*⁺ cells (arrows) using probes targeting *Grm8*, *Oprm1*, and *Chst9*. Scale bar, 10 μ m. **d**, Spatial distribution plots ($n = 5$ rats) of cells expressing *Oprm1* and *Chst9* mRNA. Scale bar, 500 μ m. Mean *Oprm1* intensity per cell is represented in the spot area. **e**, Quantification and comparison of raw *Oprm1* intensity and puncta count in *Oprm1*⁺/*Chst9*⁻ and *Oprm1*⁺/*Chst9*⁺ populations (nested t -test: $p < 0.0001$,

$p = 0.0002$). **f**, Percentage of cells positive for *Oprm1* mRNA, classified within cells labeled by other MSN markers (or all NAc cells).

Author Manuscript

Author Manuscript

Author Manuscript

Author Manuscript

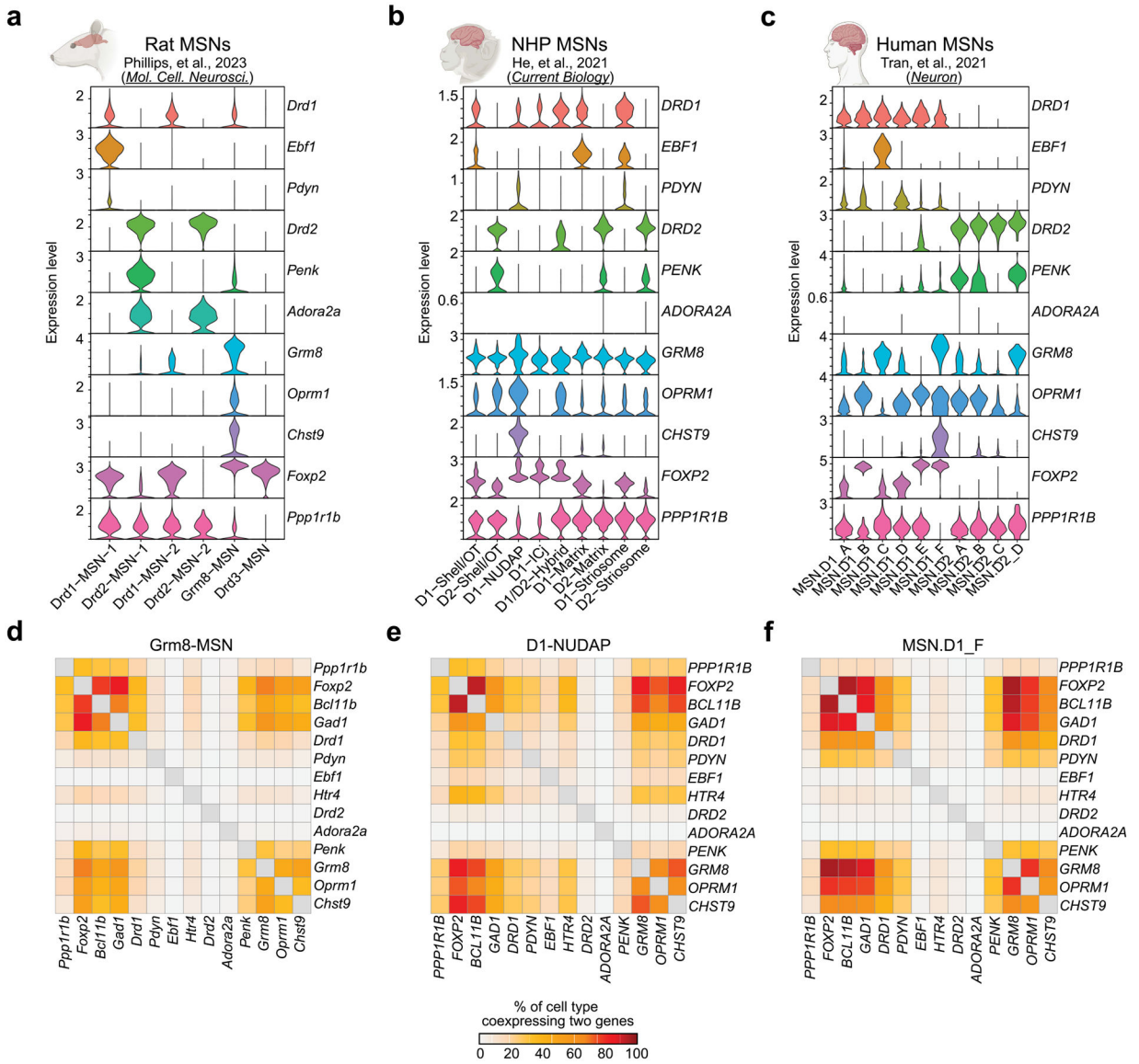


Fig. 3. Identification of conserved populations of *Chst9*⁺ neurons in non-human primates and humans. **a-c**, Violin plots of MSN marker genes in transcriptionally defined cell populations of the rat (**a**), non-human primate (**b**), and human (**c**) NAc. **d-f**, Coexpression heatmaps showing the percent of cells within the rat Grm8-MSN cluster (**d**), non-human primate D1-NUDAP cluster (**e**), or human MSN.D1_F cluster (**f**) coexpressing identified genes.